Control of composite thin film made in an Ar/isopropanol/TiO 2 nanoparticles dielectric barrier discharge by the excitation frequency

Paul Brunet, Rocío Rincón, Jean-Michel Martinez, Zineb Matouk, Fiorenza Fanelli, Mohamed Chaker, Françoise F. Massines

Article type: Full Paper

Title: Control of composite thin film made in an Ar/isopropanol/TiO_2 nanoparticles Dielectric Barrier Discharge by the excitation frequency

Paul Brunet[1, 2], Rocío Rincón[2], Jean-Michel Martinez[1], Zineb Matouk[2], Fiorenza Fanelli[3], Mohamed Chaker[2], Françoise Massines[1]

[1]Laboratoire PROcédés Matériaux et Energie Solaire, UPR 8521, Tecnosud, 66100 Perpignan, France

e-mail: françoise.massines@promes.cnrs.fr

[2]Institut National de la Recherche Scientifique, 1650 boulevard Lionel Boulet J3X1S2 Varennes, Canada

e-mail: chaker@emt.inrs.ca

[3]Institute of Nanotechnology, National Research Council (NANOTEC-CNR), c/o Department of Chemistry, University of Bari Aldo Moro, via Orabona 4, 70126 Bari, Italy

The synthesis of composites thin films made by injecting an aerosol suspension of 20 nm-size TiO_2 nanoparticles (NPs) and isopropanol (IPA) in a filamentary argon DBD (Dielectric Barrier Discharge) is studied as a function of the DBD frequency from 1 to 50 kHz. The plasma is modulated to get homogeneous coatings. The deposition rate and morphology of the composite thin films are determined from SEM images of both surface and cross section. Their chemical composition is investigated by XPS, Raman and FTIR measurements. The structural composition of the NPs is examined by XRD. All the deposited composites show the chemical signature of the NPs as well as of the polymer-like coating resulting from the plasma polymerization of IPA. No mixed phase is

observed and the sizes of the NPs as well as of their aggregates are not affected by the plasma. With this method aerosol droplets are evaporated before entering the plasma and the NPs inside a same droplet are aggregated. Results show that the DBD frequency controls the composite composition by independently influencing the NPs transport and the matrix growth rate. At 1 kHz, the coating is essentially made of NPs with a low carbon coating. From 1 to 50 kHz, the Ti/C ratio is divided by two orders of magnitude. As the frequency increases the quantity of NPs decreases and since 10 kHz the matrix thickness increases. The decrease of the NPs is explained by the numerical modeling of the NPs trajectory. It is found that from 10 to 1 kHz, the lower is the frequency, the higher is the transport of the NPs to the surface due to the electrostatic force. On the other hand the matrix growth rate increases from almost zero at 10 kHz up to 19 $nm.min^{-1}$ at 50 kHz because of the linear increases of the DBD power with the frequency.

1. Introduction:

Initially used to treat the surface of different polymers, especially to change their wettability or their adhesion [1-7], dielectric barrier discharges (DBD) are increasingly studied. New DBD operation modes allowed the deposition of organic[8-11] and inorganic thin films[12,13] as well as of homogeneous coatings on large surface that advantageously compete with those deposited in low pressure plasma conditions[14]. The DBD-based technology is industrially relevant due to its capability of performing treatments on large surfaces and of its operation at atmospheric pressure that enables to process sensitive and outgassing materials like woods[15], tissues[16,17], and alive organisms[18] that cannot be placed in low pressure environment.

Recently, a growing interest for multifunctional coatings has appeared with the development of nanocomposites thin films that consist of NPs embedded in a matrix. The presence of NPs provides the nanocomposite with extra properties related to their interactions with the matrix.[19-22] In the literature, two approaches exist for synthesizing nanocomposite thin films using atmospheric pressure DBDs. One consists in using two different precursors, one to create the NPs and the other to

deposit the host matrix.[23] The advantage of the method is that immiscible precursors can be used but it presents the disadvantage that the properties, size and shape of the NPs are difficult to control together with the interface between the matrix and the NPs.[24] A second approach consists of creating an aerosol of NPs in suspension in a polymerizable liquid and to inject it in the plasma.[19,20,25-30] As the NPs are synthesized independently of the plasma, their characteristics can be well controlled. However, as it is shown by Fanelli *et al.*[27], a suitable solvent is necessary to create an appropriate aerosol of NPs suspension. Furthermore, if the NPs are not properly functionalized, they aggregate during the evaporation of the aerosol droplet.[25,30] In the end, these aggregates are included in the matrix. This is not a drawback for applications that benefit from the strong roughness surface induced by nano/micro NPs aggregates structuring like super hydrophobic properties.[31] The size of the aggregates increase with the concentration of NPs in the suspension. However, the suspension concentration cannot be reduced considerably since it determines the NPs concentration deposited in the composite thin film.[28] Aggregates are avoided if the concentration of NPs is reduced to such a point that there is only one NP in each droplet of the aerosol. However, for most application, it induces a too low concentration of NPs in the thin film but for those which not require a high concentration of NPs in the composite it is a solution.[20]

To reduce the agglomeration phenomenon, different solutions are used. The first one consists of functionalizing the NPs. This functionalization can be steric,[30] in which long chain are grafted on the NPs surface, or electrostatic, in which ionic charges are added on the NPs to induce repulsive forces.[32] The solvent is also a key parameter to limit the agglomeration rate as shown by Dowling *et al.*[26,28] Small amounts of alcohol increase the stability of TiO_2 NPs suspensions. More generally, a small amount of a polar solvent in the suspension yields a better stability, hence a better homogeneity together with a smaller size of NPs aggregates in the coating. Moreover, using a nebulization chamber or a wall impactor[33] removes the bigger droplets and therefore the bigger aggregates. For this reason, an alcohol is chosen as solvent and polymerizable liquid in this study

which aims to contribute to a better control of the integration of NPs aggregates thanks to the electrostatic force induced by the plasma voltage.[30]

The transport of the NPs in a plasma is governed by different forces that include gravity, neutral and ion drag, thermophoresis and electrostatic forces.[34,35] The last three forces are related to the plasma characteristics. The ion drag is controlled by the ion density according to the discharge regime, while thermophoresis is related to the temperature gradients between the gas bulk and the electrodes or between different plasma regions. The electrostatic force is proportional to the electrical field and to the NPs charging that depends on the plasma regime and on the experimental configuration of the DBD (gap and shape of the dielectric). Profili *et al.*[30] have shown that gravity does not play a significant role as compared to the electrostatic force even with the plasma off. However, for a sinusoidal voltage this remains true as far as the voltage frequency is low enough to allow a NP oscillation amplitude larger than the gas gap. As investigate by Profili *et al.*[35], in the case of a Townsend discharge, an increase of the applied frequency produces the drastic decrease of the NPs concentration. Moreover it seems that in their configuration, most of the NPs are deposited before the edge of the DBD electrode due to the shape of the electric field in this area. In order to improve the substrate coverage, i.e the spatial homogeneity of the deposited NPs all along the substrate, Profili *et al.*[36] used a new complex excitation waveform where two frequencies are alternatively employed. It was shown that a homogenous Townsend discharge regime can be maintained even by injecting precursors and that a more uniform concentration of NPs can be obtained all along the substrate. In our study, the plasma is amplitude-modulated so that the plasma is ON during half the time and OFF during the other half. This amplitude modulation was shown by Vallade *et al*.[37] to be a good solution to improve the homogeneity of the deposition all along the substrate.

The present work aims to study the influence of the applied voltage frequency on the NPs oscillation amplitude in an Ar filamentary discharge and its impact on the morphology, the chemical composition and the spatial homogeneity of the coating.

The case of 20 nm size TiO_2 NPs dispersed in isopropanol (IPA) diluted in Ar at atmospheric pressure is considered. The plasma source is a DBD operated in the frequency range 1 - 50 kHz. Scanning electron microscopy (SEM) images and X-Ray Diffraction (XRD) spectra of the thin films are compared. The results are discussed in terms of simulations of NPs trajectories in the gas flow. Moreover, the growth rate of the films is compared with that achieved with IPA alone. Finally, the chemical composition of the thin films is examined.

2. Experimental setup and numerical modeling:

In this section, the procedure of preparation and of injection of TiO_2 suspension into the DBD is first described and followed by the presentation of the DBD reactor. The composite characterization methods are then briefly explained. Finally, the numerical model developed to calculate the trajectory of the NPs is overviewed.

2.1 Preparation and injection of TiO_2 nanoparticles suspension:

One percent $1\%_{wt}$ in weight of commercial TiO_2 nanoparticles (20 nm) coated by Tetramethoxysilane (Evonik) was added to 50 ml of isopropanol (IPA). The mixture was sonicated with an ultrasound tip during 20 min to minimize the size of aggregates in the suspension. During all the experiments, the suspension was magnetically stirred to avoid flocculation and sedimentation. The aerosol was formed with a pneumatic atomizer TSI (3076) using an argon flow of 1.1 $L.min^{-1}$. This gas flow is the minimum required to create a Ventury effect and thus to generate an aerosol. The gas expands through an orifice of 0.3 mm diameter to form a high-velocity jet that impacts the wall, resulting in the removal of the larger droplets. Liquid is brought from the bottle to the atomizing region through a vertical tube. The atomizer works in recirculation mode, which means that the suspension excess is drained back to the bottle. A fine spray leaves the atomizer region through a standard fitting located on the top of the atomizer. It is then diluted with an Ar flow of 3.9 $L.min^{-1}$. The suspension flow is estimated by weighting the bottle before and after each experiment. Its value is 0.2 ±0.02 $g.min^{-1}$.

2.2 Plasma reactor and depositions conditions:

A schematic drawing of the discharge cell is shown in Figure 1. It consists of two parallel dielectric plates separated by a 2 mm gap. Each electrode is fabricated by metalizing a 4x4 cm² square on the rear of a 7x7 cm² Al_2O_3 dielectric plate. The thickness of the dielectric is 1 mm for the top electrode and 635 µm for the bottom one. The substrate is made of a 2''-diameter silicon wafer of 275 µm thickness. It is held on the bottom dielectric by an alumina holder of 0.3 mm to ensure a plane surface and to avoid any gas flow perturbation. The electrodes are placed into the vacuum chamber and pumped to remove the impurities prior to the introduction of Ar up to the atmospheric pressure (760 Torr).

The Ar/TiO_2/IPA mixture is injected through a 0.1x4 cm² slit located at 4 cm ahead of the plasma. Once the gas is injected, it is guided by two quartz bars until its aspiration on the opposite side. The gas flow is laminar.

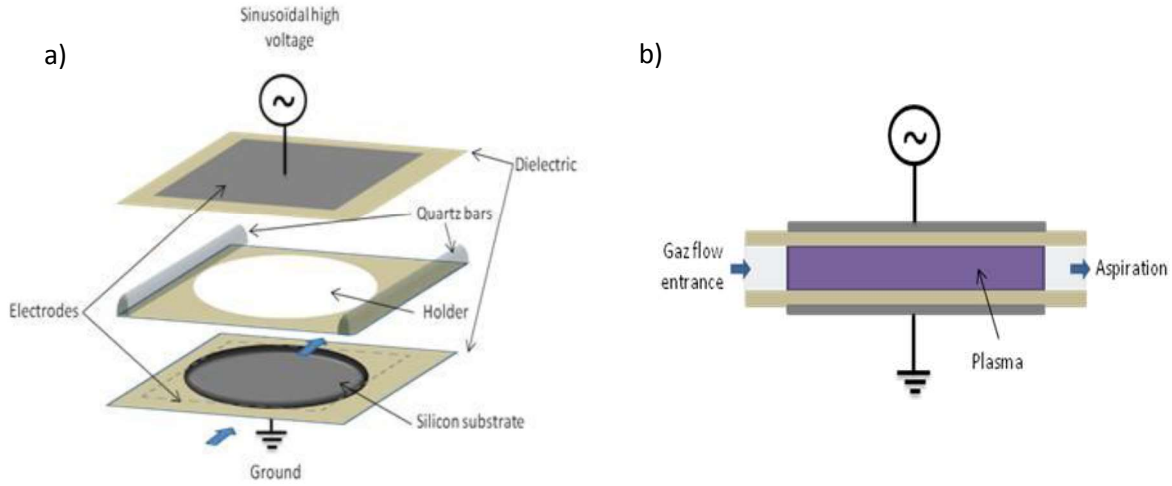

Figure 1: Schematic drawing of the discharge cell a) detailed view b) view through quartz bar

The plasma is generated in the gas gap by applying a sinusoidal high voltage (HV) to the upper electrode while the bottom one is grounded. The HV is issued from a low frequency waveform generator (Agilent 33210) connected to an audio amplifier (Crest CC4000) linked to a voltage transformer (Boige et Vignal).

In the present study, two transformers are used, one to operate from 1 to 10 kHz with a voltage ranging between 1 and 15 kV and the second from 25 to 100 kHz with a voltage ranging between 1 and 7 kV.

The voltage applied to the electrode and the current flowing in the discharge are monitored by a high voltage probe (Tektronix P6015A 1V/1000V) and a current probe (Lilco LTD 5V/A) both connected to a digital oscilloscope (Tektronix TDS2014). According to Equation 1[38], the power in the discharge is calculated from these electrical measurements as:

$$P = f\int_0^{1/f} u(t) * i(t)\, dt \qquad Equation\ (1)$$

where f is the frequency, u is the amplitude of the voltage applied to the electrode and i the current measured as closed as possible to the grounded electrode all being function of time t. In our case, the power flux is used (power divided by the surface of the electrode) to evaluate the influence of the whole plasma surface

The deposition duration is 20 min with a total Ar flow (Air Liquide Argon 2) of 5 L.min^{-1} (1.1 L.min^{-1} in the atomizer and 3.9 L.min^{-1} injected between the atomizer and the reactor to dilute the precursor and to ensure droplet evaporation before entering the plasma. The atomizeur is located at about 80 cm from the plasma entrance and the concentrations of IPA and of TiO_2 NPs in the plasma are 31500 ppm and 10^9 NPs cm^{-3} respectively. These values are calculated taking into account a suspension injection of 0.2 g.min^{-1}, a dilution gas flow of 5 L.min^{-1} and a concentration of NPs in the suspension of 10^{13} NPs cm^{-3}, which represents a 1 % weight of TiO_2 NPs in IPA.

The experimental conditions are summarized in the Table 1. Except for the last experiment ($S_{NOmod(10)}$) which is performed without modulation (plasma continuously ON), the other ones are carried out by modulating the plasma at a repetition rate of 50 Hz with a duty-cycle of 50% (the discharge is ON and OFF during 10 ms each) to achieve a homogeneous coating all along the plasma as shown by Vallade *et al.*[37]

The mean residence time of the gas and of the NPs corresponds to that needed for the suspension to travel along the 4 cm plasma zone. The residence time t_r (s) is calculated following the Equation (2)

$$tr = \frac{p_p}{F_g/A} \qquad Equation\ (2)$$

where p_p (m) is the position along the plasma in, F_g ($m^3.s^{-1}$) is the gas flow rate and A (m^2) is the cross-section through which the gas is guided. Considering a gas flow of 5 $L.min^{-1}$, a plasma length of 4.10^{-2} m, and a surface of $0.8.10^{-4}$ m^2, the total residence time is 38.4 ms. On the other hand, for a frequency modulation of 50 Hz, the duration of one modulation cycle is 20 ms, which results in about 2 plasma modulation cycles during the residence time. In every case, the voltage is kept constant at 4 kV and four different plasma excitation frequencies of 1, 10, 25 and 50 kHz are used.

Table 1: Summary of the experimental conditions

Number sample	Frequency (kHz)	Plasma power ($W.cm^{-2}$)	Precursors	Voltage amplitude (kV)	Modulation DC	Precursor Injection ($g.min^{-1}$)
$S_{IPA\ (50)}$	50	0.42	IPA	4	50 Hz 50%	0.16
$S_{IPA\ (25)}$	25	0.21				0.17
$S_{IPA\ (10)}$	10	0.08				0.156
$S_{IPA\ (1)}$	1	0.007				0.16
$S_{(50)}$	50	0.35	IPA+ TiO_2	4	50 Hz 50%	0.20
$S_{(25)}$	25	0.16				0.18
$S_{(10)}$	10	0.065				0.20
$S_{(1)}$	1	0.006				0.215
$S_{NOmod(10)}$	10	0.14	IPA+ TiO_2	4	NO	0.19

In our case, the discharge operates in the filamentary mode because the precursor percentage is high as compared to the typical maximum value in atmospheric pressure glow discharges which is typically less than 100 ppm.[39,40]

2.3 Samples characterization:

Whatever the characterization method considered, each sample is analyzed at four positions over the surface, each one corresponding to a specific distance from the edge of the DBD electrodes 0.5, 1.5, 2.5 and 3.5 cm. These positions are associated to specific mean residence times of 4.8, 14.5, 28 and 33.5 ms for the precursor in the plasma as defined by Equation (2).

The surface and cross section morphology of TiO_2 NPs plasma thin film are investigated by scanning electron microscopy (SEM Hitachi S-4500). The images are acquired in the high resolution mode with an extraction voltage of 5 kV and a magnification from x10 K to x100 K.

The chemical composition of the coating is analyzed by X-ray photoelectron spectroscopy (VG Escalab 220i XL) using a 1486.6 eV, Al Kα X-ray source. Survey (0–1400 eV) and high resolution (C1s, O1s, Ar2p, Si2p and Ti2p) spectra are recorded. The atomic percentage of each element is determined from the high resolution spectra with the CasaXPS software after calibration of the binding energy by using the carbon C1s peak at 285 eV corresponding to the hydrocarbon (C-C/C-H).

Fast Fourier Transform Infra-Red spectroscopy analysis is carried out in the transmission mode (Nicolet 6700 thermo scientific). A background for the silicon wafer alone is carried out for each experiment. The baseline is subtracted after each experiment by determining a linear baseline with the Omnic software in a spectral area free of peaks. The spectrometer is flushed with dry air and acquisition is achieved when the CO_2 peak between 2345-2600 cm^{-1} (3846 - 4264 nm) is close to 0.

Raman spectroscopy is performed with a Horiba Jobin Yvon LabRAM ARAMIS IR^2 system equipped with a red laser at 633 nm wavelength, a CCD detector and an edge filter to acquire only the anti-Stokes shift.

2.4 Numerical simulation of NPs trajectory:

As already mentioned, once NPs are introduced inside the plasma, they are submitted to five forces[41], namely the electrostatic, thermophoresis, ion drag, gravity and neutral drag forces. In the plasma used in this study, the neutral atom temperature is close to the room temperature and the ionization degree is very low. Thus, the ion drag and thermophoresis forces are negligible as compared to the electrostatic and neutral drag forces.[41,42] This simplify model was actually inspired from reference[35]. However, in our case, the NPs are bigger than in reference [35] (> 100 nm). Therefore, we believe that the simulations are of strong interest to take into account the aggregation of the NPs contained in the droplets after atomization. The gas flow is laminar, thus the gas velocity profile is taken as parabolic as shown in Figure 2.[43]

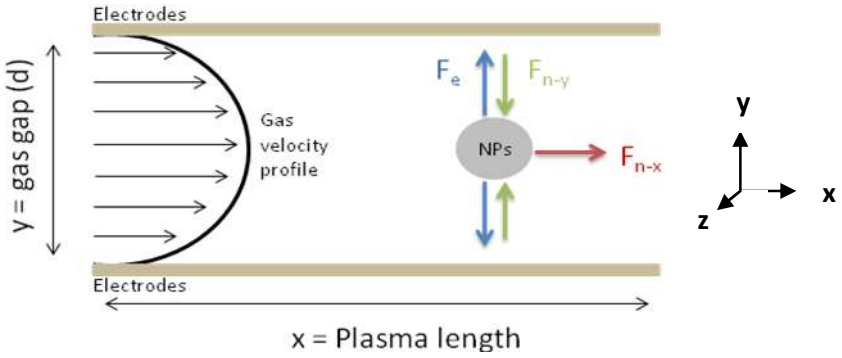

Figure 2: schematic representation of the gas flow profile between the electrodes and the forces considered for the trajectory calculation: Fe is the electrostatic force, F_{n-x} the neutral drag force on x and F_{n-y} the neutral drag force on y

The electrostatic force is expressed as Equation 3:

$$F_E = Q.E \qquad Equation\ (3)$$

Where, Q is the total number of charges of a particle and E is the electric field determined by the voltage V across the gas gap d. According to the literature, we assume that the charge of a 100 nm NP is Q = -100. [44]

The projection of the neutral drag force on the x and y axes is expressed by Equation (4) and (5):

$$F_{n-x} = 6\pi\eta r_p \left(v_g - v_x\right) \qquad Equation\ (4)$$

$$F_{n-y} = 6\pi\eta r_p \left(v_y\right) \qquad Equation\ (5)$$

where η is the gas viscosity, r_p the particles radius, v_g the gas velocity, v_x and v_y the particles velocity along the x axis and the y axis respectively.

Considering the fundamental principle of dynamics:

$$m_p \frac{d\vec{v}}{dt} = \sum \vec{F}$$

One can write Equation (6) and (7):

$$\frac{d^2y}{dt^2} + K_1\frac{dy}{dt} = K_2\, cos\,(\omega t + \chi) \qquad Equation\ (6)$$

$$\frac{d^2x}{dt^2} + K_1\frac{dx}{dt} = \frac{6K_1\bar{V}}{d^2}y(d-y) \qquad Equation\ (7)$$

with $K_1 = \frac{6\pi\eta r_p}{m_p}$ and $K_2 = \frac{Q.E}{m_p}$

Solving the Equations (6) and (7) yields a parametric equation for x(t) and y(t) thanks to Laplace transformation Equation (9) and (8) respectively, i.e.

$$y(t) = \frac{K_2}{\omega^2 + {K_1}^2}\left[\left(\frac{\omega}{K_1}\sin(\chi) + cos(\chi)\right)e^{-K_1 t} + \frac{K_1}{\omega}\sin(\omega t + \chi) - cos(\omega t + \chi)\right]$$

$$-\frac{K_2}{\omega K_1}\sin(\chi) + y_0 \qquad Equation\ (8)$$

$$x(t) = \int_0^t \left[\frac{\int_0^\tau \frac{6\bar{V}}{d^2}y(\theta)[d - y(\theta)]e^{K_1\theta}d\theta}{e^{K_1\tau}}\right]d\tau \qquad Equation\ (9)$$

Equation (9) enables to determine the position of the NPs across the gas gap and along the plasma at a given time, which yields the NPs trajectory.

3. Results and discussion:

In this section, the effect of the Ar DBD frequency on the morphology of the composite thin film is firstly presented and discussed on the basis of SEM images, XRD measurements and NPs trajectory modeling. Secondly, the variation of the chemical composition is presented. The discussion aimed to determine the mechanisms that are responsible for the composite thin film morphology.

3.1 Morphology of the thin film coatings:

After a description of the composite thin films synthesized with a DBD operated at 1 and 50 kHz, the main mechanisms controlling the NPs inclusion and the matrix growth are discussed.

3.1.1: Comparison of the coatings obtained in DBDs operated at 1 and 50 kHz modulated at 50 Hz:

The typical morphology of the coatings grown with IPA and TiO_2 NPs is compared in Figure 3. SEM images of both surfaces and cross-sections are presented for a DBD operated at frequencies of 1 kHz (Figure 3a) and 50 kHz (Figure 3b). Regardless of the frequency, the NPs agglomerates have a typical size in the micrometer range and unfortunately most of the nanoparticles are aggregated. No nanoparticles with their initial size were detected by SEM cross section neither in the matrix nor at the surface. A previous work[45] has shown that this size is determined by the dimension of the aerosol droplet. All the NPs contained in one droplet form an aggregate when IPA evaporates in the gas line before the interaction between the NPs and the plasma. A wafer positioned at the gas flow entrance did not collect droplets, which confirms that most of IPA is evaporated in this point. Two main differences occur for the thin films deposited at 1 and 50 kHz: (i) the quantity of NPs deposited and (ii) the appearance of the aggregates.

At 1 kHz, the coating is mainly formed by NPs agglomerates. In addition, the 20 nm-size NPs are clearly observable within the aggregates. In contrast, at 50 kHz, fewer particles are spread over a dense coating and the 20 nm structure disappears.

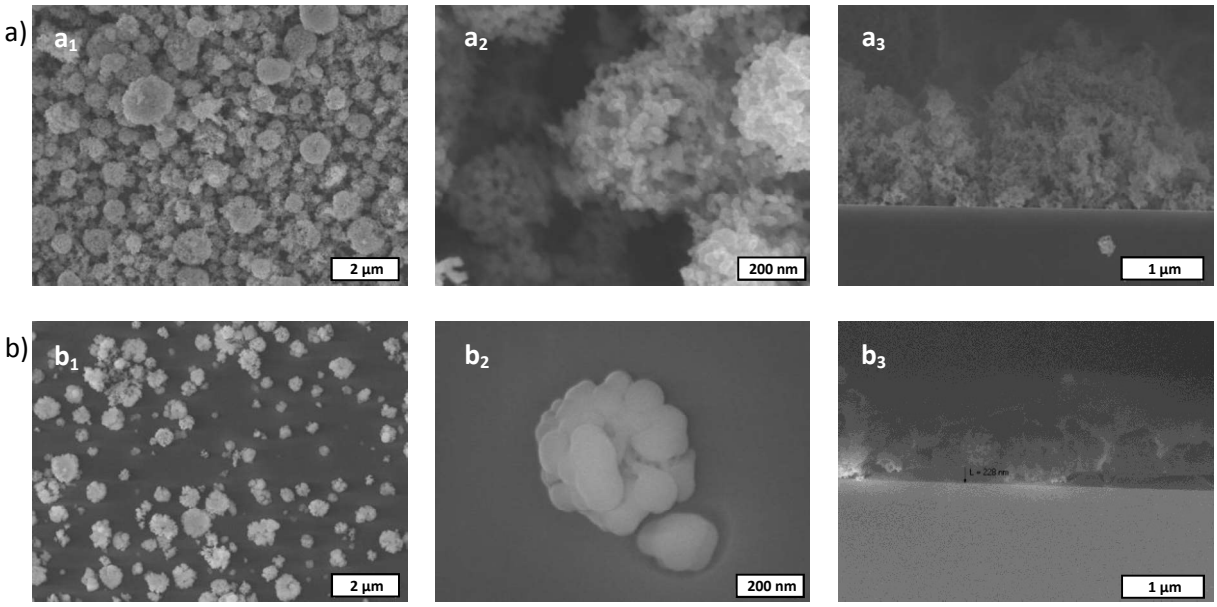

Figure 3: SEM surface and cross section a) $S_{(1)}$ b) $S_{(50)}$

X-ray diffraction was performed to determine the possible presence of the 20 nm NPs in the agglomerate. The results are shown in Figure 4 for the different frequencies. The main crystalline orientation corresponding to anatase TiO_2 (101-004-200-105-211-204-116-220-215) and rutile TiO_2 (110) phases are observed as in the original powder (20% Rutile and 80% Anatase). The decrease of the peak intensity is not related to a decrease of the crystallinity but rather to that of the NPs concentration on the sample as observed on the SEM pictures. The crystallite size is deduced from XRD spectra using Sherrer's relation showed in Equation (10).

$$\boldsymbol{D = \frac{0.9\,\lambda}{\beta \cos\theta}} \qquad Equation\ (10)$$

Where, D is the crystallite average size, λ is the X-ray wavelength (0.154 nm), θ is the Bragg diffraction angle and β is the FWHM.

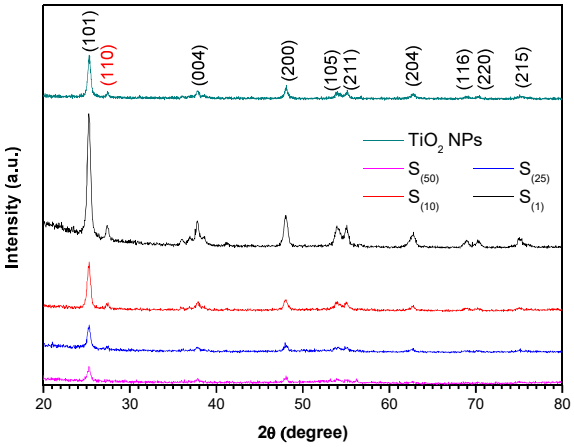

Figure 4 XRD spectra of pristine TiO_2 and of the deposition in the entrance (0.5 mm) for the different frequencies: $S_{(1)}$, $S_{(10)}$, $S_{(25)}$ and $S_{(50)}$ samples

For every sample, the size of the crystallite determined by Equation (10) is about 25 nm regardless of the plasma conditions. This value stands close to the 20 nm size defined by the manufacturer. This means that the plasma weakly influences the NPs size. The 20 nm structure observed on the SEM images at 1 kHz and not at 50 kHz is not due to a modification of the NPs but rather results from the coating of the NPs aggregates stemming from the precursor in the gas bulk and at the surface. In Figure 3, one observes the initial size of the NPs which is 20 nm (see Figure 3 image a2). In the other case, (Figure 3 image b2), the size looks larger due to the coating of the aggregate resulting from IPA polymerization in the discharge. This effect was previously observed for ZnO using n-octane as liquid precursor.[27] To better analyze and understand these observations, the concentration of NPs and the thickness of the matrix in the coatings are compared for the different frequencies (1, 10, 25 and 50 kHz).

3.1.2: NPs concentration in the coatings:

The NPs density was estimated from the SEM pictures by calculating the ratio between the surface covered by NPs and the total surface. This ratio was measured at different residence times of the precursor in the plasma.

For each position along the x-axis, three measurements over the z-axis are performed, i.e. for a same position on the wafer. The surface coverage by NPs was determined with the ImageJ software. The results are presented in Figure 5 as a function of the mean gas residence time. The errors bars are estimated from the average of the three measurements over the z-axis. At 1 kHz ($S_{(1)}$), the whole substrate is covered by the NPs all along the plasma. The transfer of NPs to the substrate is very efficient. As it shown, for a 10 kHz ($S_{(10)}$) frequency a better substrate coverage all along the substrate is reached with an amplitude modulation than without ($S_{NOmod(10)}$) which results in a higher concentration in the case of modulation.

At higher frequencies, a drastic decrease of NPs occurs at the plasma entrance (5 mm, 5 ms). For the other positions, the NPs coverage becomes independent of the plasma position with a value around 40%.

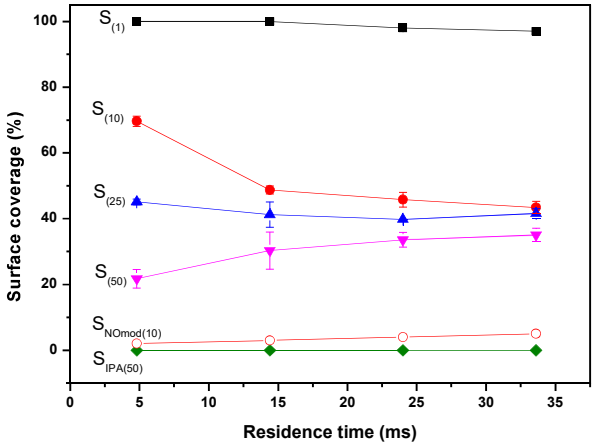

Figure 5: Percentage of the coverage by NPs as a function of the frequency ($S_{(1)}$, $S_{(10)}$, $S_{(25)}$, $S_{(50)}$, $S_{NOmod(10)}$ and $S_{IPA(50)}$ samples)for different residence times of the precursor in the plasma

Modeling was used to determine whether or not the electrostatic force exerted on the NPs could explain the experimental observations. Assuming that the NPs velocity is the same as the gas velocity, $F_{n\text{-}x}$ (Figure 2) is equal to 0. Therefore, the NPs velocity remains constant along x.

This velocity is maximum in the center of the gap (1.5 $m.s^{-1}$) and reaches 0 on the surface according to the parabolic variation along y. The sinusoidal electric field is assumed to be uniform in the entire gas gap. Its amplitude is 10 $kV.cm^{-1}$ (2 kV across the 2 mm gap) and the voltage modulation is not considered. Since electron velocity is largely higher than ion's ones we considered here a total negative fixed charge of 100 on each 100 diameter aggregates. Figure 6 presents the calculated trajectory of a NP for the different frequencies considered in the experimental section. As the applied voltage is sinusoidal, it induces NPs oscillations with amplitudes of 600, 60, 22 and 10 µm at 1, 10, 25 and 50 kHz respectively.

Therefore, the amplitude falls by a factor of 60 as the frequency increases from 1 to 50 kHz which is in agreement with the previously experimental observations i.e. higher is the frequency, lower is the NPs deposited concentration.

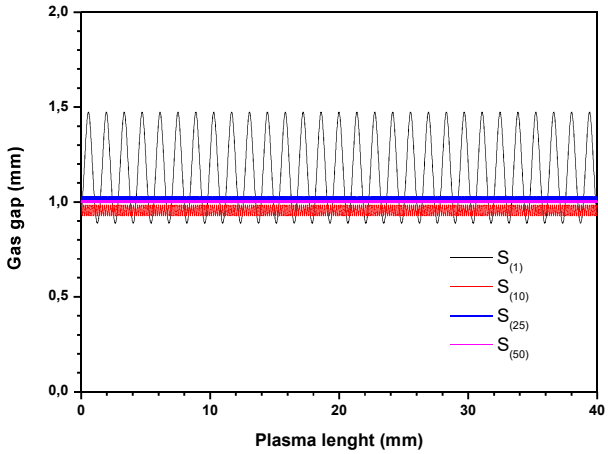

Figure 6: Numerical simulation of the trajectory of NPs in the plasma

According to the numerical simulation, the NPs are able to be deposited on the substrate if two conditions are gathered. First, the NPs should enter in the gas gap at a shorter distance from the substrate than their amplitude oscillation.

Second, since the voltage is alternative if the distance to the surface is equal to their oscillation amplitude they should enter in the discharge when the voltage is decreasing to reach the substrate due to electrostatic force.

As shown, for 1 kHz NPs should enter at a distance shorter than 0.6 mm (corresponding to their maximum amplitude oscillation) from the substrate and the voltage should decrease to have a chance to reach the substrate. For 10 kHz, they should enter the gas gap at a distance to the substrate shorter than 60 µm. In this case this distance is shorter than the usual limit layer defined by the diffusion which is of the order of 100 µm in similar conditions.[39]

Thus, for the gas flow, gas gap, voltage amplitude and frequencies used in this study, the electrostatic force is found to significantly participate to the transport of NPs to the surface when the frequency is equal to or lower than 1 kHz. This explains the large surface coverage at 1 kHz observed in Figure 5. At 10 kHz and higher frequency, the NPs are trapped in the gas, which yields the drastic decrease of NPs concentration in the coating between 1 and 10 kHz.

Nevertheless Figure 3 b1 shows that even at 50 kHz in our conditions some NPs are present in the coating. This is due to the plasma modulation, that is not considered in the numerical simulation, as the plasma is alternatively on and off during 10 ms. Since the gas residence time in the plasma is 38.4 ms, the NPs are submitted to about two modulation cycles during their transport along the plasma. When the plasma is on, most of the NP_S are trapped. As soon as the plasma is turned off, a constant electric field due to the charge accumulated on the dielectric surfaces takes place, which drives the particles to the surface and therefore explains the presence of NPs in the thin film. This can be understood by comparing coating without (Figure 7 a) and with modulation (Figure 7 b) for a frequency of 10 kHz. Even if the discharge works in filamentary regime, the results show the same effects as the investigation conducted by Profili *et al.*[35] in Townsend regime.

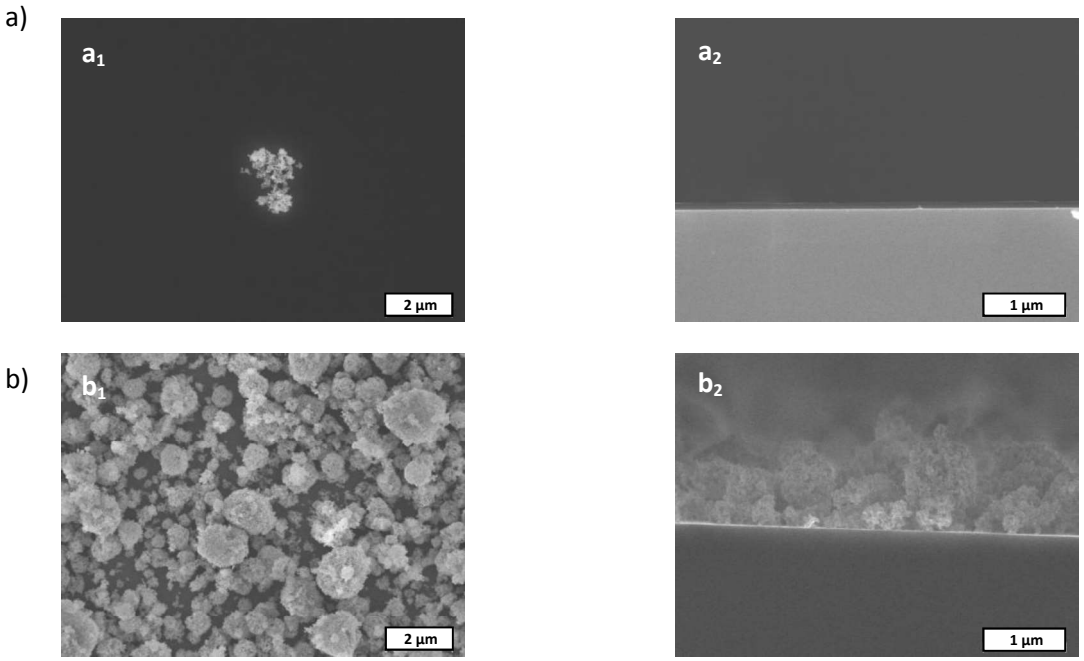

Figure 7: SEM surface and cross section a) $S_{nomod(10)}$ and b) $S_{(10)}$

As predicted, few NPs are observed on the surface or cross section without modulation and some of them deposited can even be attributed to contamination at the end of the plasma.

3.1.3: Matrix thickness:

Due to the modulation NPs are always incorporated in the coating. From the cross section SEM images, one can determine the NPs thickness of the thin film as well as the thickness of the dense layer due to IPA polymerization. The latter is measured from images free of NPs. The total thickness represents the sum of both contributions, i.e, the thickness related to the NPs deposited and the thickness related to the polymerization of isopropanol. The results are presented in Figure 8. The total thickness decreases when the frequency increases because of the incorporation of NPs in the coating is reduced. This result is in agreement with our previous analysis of the effect of electrostatic forces on NPs transport. It is important to emphasize that the thickness due to NPs decreases from the entrance to the exit from the plasma region, a feature enhanced at low frequency. As shown for frequency lower than 10 kHz no matrix is observable.

This is true when IPA and NPs are injected in the plasma but also when IPA alone is injected. In both cases, for frequency higher than 10 kHz the matrix start growing and for 50 kHz the growth rate is equal to 19 nm.min^{-1} and the film is dense.

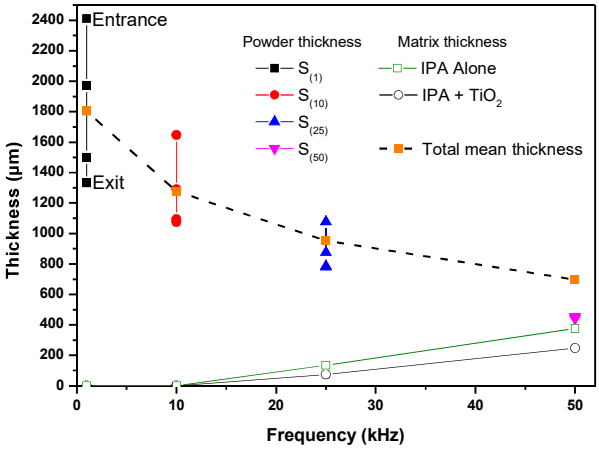

Figure 8: Thickness of the matrix without NPs (open square), thickness of the matrix with NPs (open circle), NPs thickness deposited (Full square $S_{(1)}$, circle $S_{(10)}$, up triangle $S_{(25)}$ and down triangle $S_{(50)}$) for all the position and total mean thickness matrix+TiO_2 NPs (dashed line)

The large variation of the matrix growth rate with an increase of the frequency is related to the linear discharge power augmentation with the frequency as shown in Figure 9. The power is obtained by Equation 1. This linear variation as a function of the frequency has been already observed.[46]

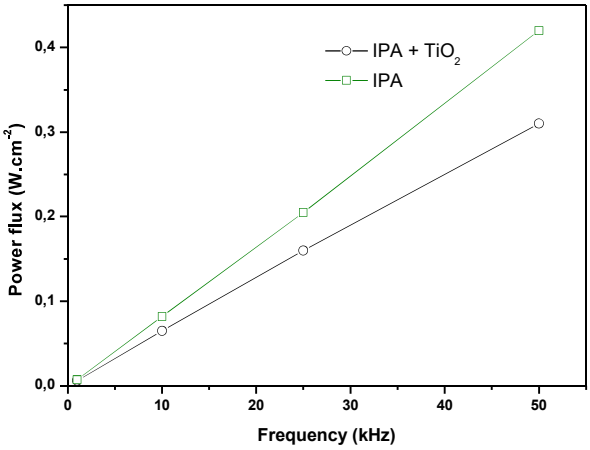

Figure 9: Power flux of the discharge as a function of the plasma frequency in Ar/IPA and Ar/IPA/TiO_2 mixtures.

The power increases with the frequency and it is lower when NPs are added to IPA and injected in the plasma: 8.2 $mW.kHz^{-1}.cm^{-2}$ for IPA alone as compared to 6.4 $mW.kHz^{-1}.cm^{-2}$ for IPA + TiO_2. The difference between IPA and IPA + TiO_2 could result from the charging of the NPs which increases electron losses and thus reduces the discharge power. As shown in Figure 10 the tendency of the matrix growth rate as a function of the power is the same with and without NPs. In both cases, matrix starts growing after 10 kHz with a power about 82 $mW.cm^{-2}$. However, the slopes are lower with NPs 44.2 $nm.cm^2.min^{-1}.W^{-1}$ compare to 55.7 $nm.cm^2.min^{-1}.W^{-1}$.

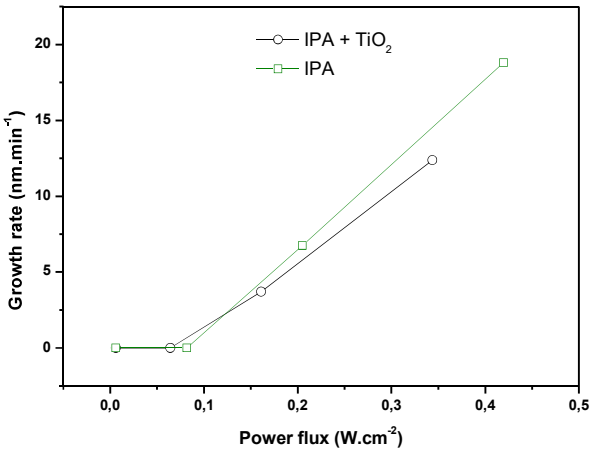

Figure 10: Growth rate as a function of the discharge power flux for IPA alone (open circle) and IPA + TiO_2 (open square)

This difference is attributed to the precursor consumption by the NPs coating which increases similarly than the matrix.

3.2 Chemical composition of the composite thin films:

The effect of the frequency on the chemical composition of the thin film is compared on the basis of XPS, FTIR and Raman measurements.

3.2.1. XPS:

Thin films were analyzed with XPS to determine the concentration of each element related to the composite. In order to remove any surface contamination all samples were etched during 360 s. Table 2 presents the average chemical composition measured at four positions over each sample.

Table 2: Chemical composition of the samples analyzed by XPS

Condition	C	O	Ar	Si	Ti
$S_{IPA(50)}$	92.8	7.2			
TiO_2 NPs	32.2	47.3		2.2	18.3
$S_{(1)}$	6.7	64	1.6	4.5	23.2
$S_{(10)}$	14.5	49.8	1.3	19.8	14.6
$S_{(25)}$	76.2	19.1	0.4		4.3
$S_{(50)}$	91.4	8.1			0.5

The layer deposited by decomposition of IPA only contains carbon and a few oxygen atoms. The TiO_2 NPs contains a large quantity of carbon, with a ratio of O/Ti of 2.5 which is likely coming from the NPs surface contamination. This value is in agreement to what has been observed in the literature.[47] The 2% of Si is probably due to the NPs functionalization achieved by the organosilane pretreatment. Ar and Si are detected at for 1 and 10 kHz, when the carbon layer is not significant. The increase of Si in the deposit can be explained by the use of a silicon wafer substrate and the low matrix thickness. The C contribution comes from the decomposition of IPA in the plasma. The drastic carbon concentration increases between 10 and 25 kHz coincides with the beginning of an efficient polymerization of IPA. At a frequency above 10 kHz, the concentration of TiO_2 in the substrate falls below 5% and even below 0.5% at 50 kHz. These very low values are in contradiction to the percentage of NPs observed on the surface sample and are explained by the presence of the polymer film coating the TiO_2 NPs aggregates at 25 and 50 kHz.

The Ti percentage varies by a factor 50 and the C concentration by a factor of 15 as the frequency varies from 1 to 50 kHz. In Figure 11, the ratio Ti/C that represents the contribution ratio between the NPs and the matrix is plotted as a function of the energy density (Power multiplied by the gas residence time in the discharge) for all the frequencies. Two behaviors are observed.

First, an exponential decay occurs due to the balance between the NPs transport to the surface and the coating growth rate. Second, jumps appear for the different frequencies. They are related to the increase of NPs contribution.

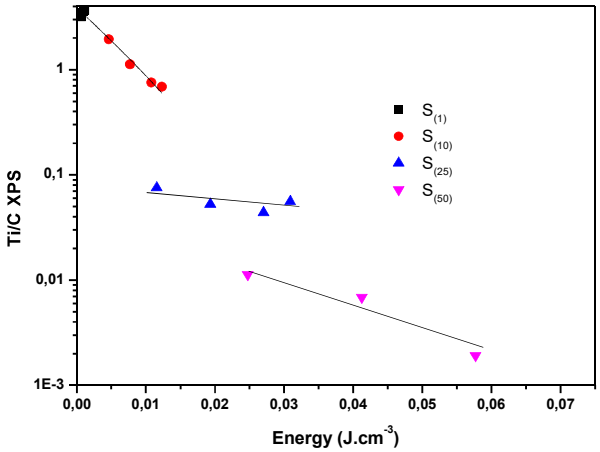

Figure 11: Ti/C ratio from XPS analysis as function of the plasma energy $S_{(1)}$ (square), $S_{(10)}$ (Circle), $S_{(25)}$ (up triangle) and $S_{(50)}$ (down triangle).

At 10 kHz, the exponential decay is due to the contribution of the TiO_2 alone because the precursor is not significantly decomposed. At 25 and 50 kHz, less and less NPs are deposited while IPA decomposition is more and more efficient as energy grows. This is accompanied by an increase of the C content in the coating and a decrease of the Ti content.

3.2.2 FTIR:

To support XPS observations, additional ATR-FTIR measurements were performed at the same positions over the samples. In Figure 12 a), the FTIR spectra obtained for TiO_2 NPs, $S_{(1)}$, $S_{(10)}$, $S_{(25)}$, $S_{(50)}$ and $S_{IPA(50)}$ are shown. Whatever the frequency, they present two broad absorption areas. One, in the range from 400 to 1000 cm^{-1} correspond to the TiO_x absorptions, with a peak at 436 cm^{-1} attributed to Ti-O bonds while the one around 678 cm^{-1} is related to symmetric O-Ti-O.[48] The second absorption area, from 2775 to 3075 cm^{-1}, is related to hydrocarbon groups.

The peaks at 2878, 2932 and 2968 cm^{-1} correspond of C-H stretches. Other peaks are present in the spectra for frequency above 25 kHz. At 1377 cm^{-1} and 1457 cm^{-1} corresponding to CH_3 and CH_2 bending respectively and OH bonded in the 3200-3550 cm^{-1} range. These peaks are clearly identified to belong to IPA. The peak at 1695 cm^{-1} is attributed to C=O. As this bound is not initially present in IPA molecule, it is related to the decomposition and polymerization of IPA by plasma when the frequency is strong enough.

The evolution of the Ti-O and O-Ti-O absorptions integrated from 400 to 1000 cm^{-1} and the one of C-H_x from 2775 to 3075 cm^{-1} are reported in Figure 12 b) as a function of the frequency. The evolution of the Ti-O bond clearly evolves similarly to Ti concentration measured by XPS with a drastic decrease up to 10 kHz. The hydrocarbons present in the FTIR spectra result of the IPA polymerization during the plasma process. They increase starts for a frequency above 10 kHz.

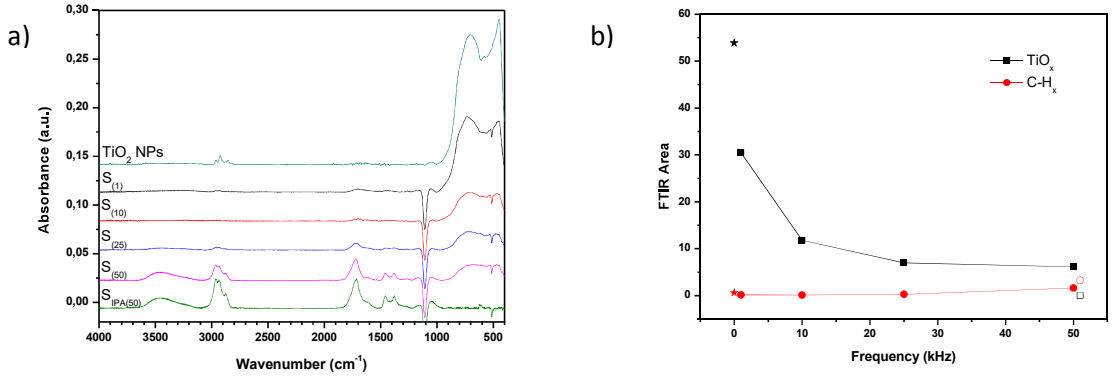

Figure 12: a) FTIR spectra, intensity as function of the wavenumber for pristine TiO_2, $S_{(1)}$, $S_{(10)}$, $S_{(25)}$, $S_{(50)}$ and $S_{IPA(50)}$ b) Area of Ti region (squares) and hydrocarbons region (circles), pristine TiO_2 (stars) and $S_{IPA(50)}$ (open symbols)

Thus, FTIR measurements confirm that increasing the frequency yields an enhancement of the matrix thickness and a decrease of the NPs in the thin film. This is also in agreement with the measurement of the mean thickness from SEM cross section pictures shown in the Figure 8.

3.2.3 Raman spectroscopy:

Raman analysis was performed to further improve the characterization of the TiO_2 NPs composites. The results are presented in Figure 13. Two peaks are observed, one at 144 cm^{-1} that corresponds to the raman vibration mode Eg of Anatase TiO_2 and another one at 520 cm^{-1} due to the Si contribution from the substrate. No other peaks can be seen in this configuration because the detector is saturated by the signal of the substrate as the coating thickness is too thin. Therefore, neither C-H nor C-C can be observed. By increasing the frequency, the Ti peak decreases while the Si peak increases due to the decrease of the total thickness. Figure 14 shows the area of the Ti peak at each position and each frequency as a function of the thickness of the NPs layer deduced from SEM. For a thickness larger than 1 µm, the Raman signal is proportional to the NPs layer thickness. However, at lower thickness, the surface is not fully covered by NPs and the signal is then predominantly governed by the Si signal coming from the substrate.

The Ti area signal of Raman spectra is directly related to the NPs thickness (Figure 8) if the NPs covered all the substrate as it is the case for frequencies lower than 10 kHz.

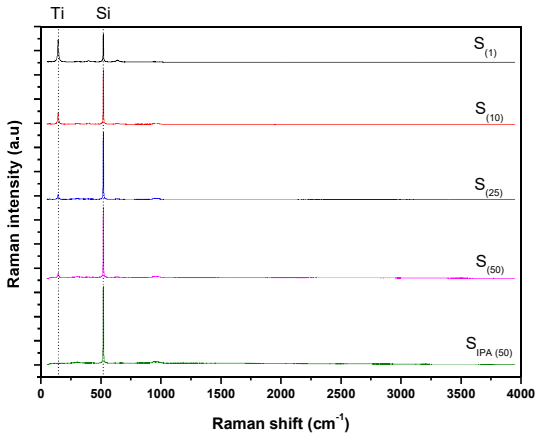

Figure 13: Raman spectra, intensity as function of the Raman shift for $S_{(1)}$, $S_{(10)}$, $S_{(25)}$, $S_{(50)}$ and $S_{IPA(50)}$ from top to down respectively

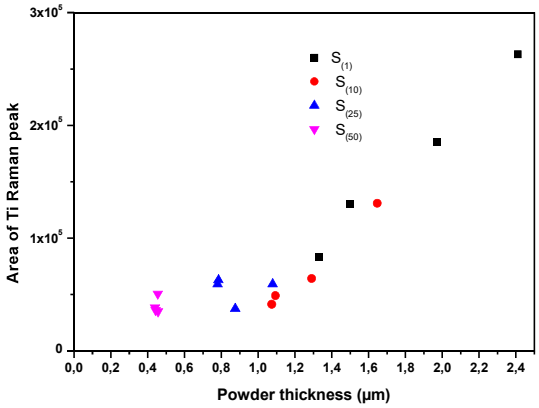

Figure 14: Ti Raman analysis as function of the powder thickness $S_{(1)}$, $S_{(10)}$, $S_{(25)}$ and $S_{(50)}$

Since all the measurements are performed under the same experimental conditions, it results in a higher concentration on NPs in the substrate when the frequency decreases.

4 Conclusion:

The increase of the frequency from 1 to 50 kHz in a DBD generated in Ar/IPA/TiO_2 mixtures in the presence of NPs has two major effects. First, the control of the NPs transport to the surface. Without the plasma modulation, between 1 and 10 kHz the consequence of the electrostatic force changes from an efficient drift to the surface to an efficient trapping in the gas bulk. Second, an increase of the discharge power and thus of IPA polymerization. A thin film growth threshold is observed around 0.1 $W.cm^{-2}$ ie 0.5 $W.cm^{-3}$. It is reached between 10 kHz and 25 kHz. At 10 kHz, the thin film is essentially made of NPs with a limited polymer matrix, while at 25 kHz and 50 kHz, it is mainly composed of the polymer matrix with an average thickness of 74 ±12 nm and 251 ±21 nm respectively. For each frequency, the maximum and minimum thicknesses are obtained respectively at the plasma entrance and at the exit.

The chemical composition of the polymer is confirmed by complementary analysis given by XPS, Raman and FTIR characterization. The NPs are only deposited when the plasma is modulated and they are coated by a polymer film.

Acknowledgements:

This work was funded by the "Agence Nationale de la Recherche" (project ANR -11- IS09 -0005) and by the National Science and Engineering Research Council (NSERC) of Canada. The authors are grateful to Emmanuel Hernandez from PROMES-CNRS and Etienne Charette from INRS-EMT for their technical involvement in the development of the DBD reactor and for their useful suggestions during the experiments.

Keywords: Dielectric Barrier Discharge (DBD); Atmospheric pressure plasma; Excitation frequency; TiO_2 nanoparticles; Nanocomposites.

[1] Massines, F.; Gouda, G. *J. Phys. D: Appl. Phys.* **1998**, *31*, 3411.
[2] Massines, F.; Gouda, G.; Gherardi, N.; Duran, M.; Croquesel, E. *Plasmas Polym.* **2001**, *6*, 35.
[3] Massines, F.; Messaoudi, R.; Mayoux, C. *Plasmas Polym.* **1998**, *3*, 43.
[4] Morent, R.; De Geyter, N.; Trentesaux, M.; Gengembre, L.; Dubruel, P.; Leys, C.; Payen, E. *Plasma Chem. Plasma Process.* **2010**, *30*, 525.
[5] Sarra-Bournet, C.; Turgeon, S.; Mantovani, D.; Laroche, G. *Plasma Process Polym* **2006**, *3*, 506.
[6] Sarra-Bournet, C.; Turgeon, S.; Mantovani, D.; Laroche, G. *J. Phys. D: Appl. Phys.* **2006**, *39*, 3461.
[7] Van Deynse, A.; Cools, P.; Leys, C.; De Geyter, N.; Morent, R. *Appl. Surf. Sci.* **2015**, *328*, 269.
[8] Truica-Marasescu, F.; Girard-Lauriault, P.-L.; Lippitz, A.; Unger, W. E. S.; Wertheimer, M. R. *Thin Solid Films* **2008**, *516*, 7406.
[9] Girard-Lauriault, P.-L.; Desjardins, P.; Unger, W. E. S.; Lippitz, A.; Wertheimer, M. R. *Plasma Process Polym* **2008**, *5*, 631.
[10] Petersen, J.; Fouquet, T.; Michel, M.; Toniazzo, V.; Dinia, A.; Ruch, D.; Bomfim, J. A. S. *ACS Applied Materials & Interfaces* **2012**, *4*, 1072.
[11] Fanelli, F.; Fracassi, F.; d'Agostino, R. *Plasma Process Polym* **2005**, *2*, 688.
[12] Maechler, L.; Sarra-Bournet, C.; Chevallier, P.; Gherardi, N.; Laroche, G. *Plasma Chem. Plasma Process.* **2011**, *31*, 175.
[13] Vangeneugden, D.; Paulussen, S.; Goossens, O.; Rego, R.; Rose, K. *Chem. Vap. Deposition* **2005**, *11*, 491.
[14] Massines, F.; Sarra-Bournet, C.; Fanelli, F.; Naudé, N.; Gherardi, N. *Plasma Process Polym* **2012**, *9*, 1041.
[15] Levasseur, O.; Stafford, L.; Gherardi, N.; Naudé, N.; Beche, E.; Esvan, J.; Blanchet, P.; Riedl, B.; Sarkissian, A. *Surf. Coat. Technol.* **2013**, *234*, 42.
[16] Borcia, G.; Anderson, C. A.; Brown, N. M. D. *Surf. Coating Tech.* **2006**, *201*, 3074.

[17] Morent, R.; De Geyter, N.; Verschuren, J.; De Clerck, K.; Kiekens, P.; Leys, C. *Surf. Coat. Technol.* **2008**, *202*, 3427.
[18] Favia, P.; Pignatelli, D.; Dilecce, G.; Pistillo, B. R.; Nardulli, M.; Gristina, R. *MRS Proceedings* **2012**, *1469*.
[19] Bardon, J.; Bour, J.; Del Frari, D.; Arnoult, C.; Ruch, D. *Plasma Process Polym* **2009**, *6*, S655.
[20] Del Frari, D.; Bour, J.; Bardon, J.; Buchheit, O.; Arnoult, C.; Ruch, D. *Journal of Nanoscience and Nanotechnology* **2010**, *10*, 2611.
[21] Beier, O.; Pfuch, A.; Horn, K.; Weisser, J.; Schnabelrauch, M.; Schimanski, A. *Plasma Process Polym* **2013**, *10*, 77.
[22] Profili, J.; Levasseur, O.; Koronai, A.; Stafford, L.; Gherardi, N. *Surf. Coat. Technol.* **2017**, *309*, 729.
[23] Rahman, M.; Amsarani, R.; Mooney, D. A.; MacElroy, J. M. D.; Dowling, D. P. *Journal of Nanoscience and Nanotechnology* **2009**, *9*, 3506.
[24] Shelemin, A.; Choukourov, A.; Kousal, J.; Slavínská, D.; Biederman, H. *Plasma Process Polym* **2014**, *11*, 864.
[25] Fanelli, F.; Fracassi, F. *Plasma Chem. Plasma Process.* **2014**, *34*, 473.
[26] Dembele, A.; Rahman, M.; Reid, I.; Twomey, B.; MacElroy, J. M. D.; Dowling, D. P. *Journal of Nanoscience and Nanotechnology* **2011**, *11*, 8730.
[27] Fanelli, F.; Mastrangelo, A. M.; Fracassi, F. *Langmuir* **2014**, *30*, 857.
[28] Denis, D. P.; Barry, T.; Gerry, B. *Journal of Nanoscience and Nanotechnology* **2010**, *10*, 2746.
[29] Michel, M.; Bour, J.; Petersen, J.; Arnoult, C.; Ettingshausen, F.; Roth, C.; Ruch, D. *Fuel Cells* **2010**, *10*, 932.
[30] Profili, J.; Levasseur, O.; Blaisot, J.-B.; Koronai, A.; Stafford, L.; Gherardi, N. *Plasma Process Polym* **2016**, n/a.
[31] Jana, S.; Mitra, B. C.; Bera, P.; Sikdar, M.; Mondal, A. *J. Alloys Compd.* **2014**, *602*, 42.
[32] Janiak, C. *Zeitschrift Fur Naturforschung Section B-a Journal of Chemical Sciences* **2013**, *68*, 1059.
[33] Fanelli, F.; Mastrangelo, A. M.; De Vietro, N.; Fracassi, F. *Nanoscience and Nanotechnology Letters* **2015**, *7*, 84.
[34] Watanabe, Y. *J. Phys. D: Appl. Phys.* **2006**, *39*, R329.
[35] Jacopo, P.; Simon, D.; Olivier, L.; Nicolas, N.; Antoine, B.; Luc, S.; Nicolas, G. *J. Phys. D: Appl. Phys.* **2017**, *50*, 075201.
[36] Profili, J.; Levasseur, O.; Naudé, N.; Chaneac, C.; Stafford, L.; Gherardi, N. *J. Appl. Phys.* **2016**, *120*, 053302.
[37] Vallade, J.; Bazinette, R.; Gaudy, L.; Massines, F. *J. Phys. D: Appl. Phys* **2014**, *47*.
[38] Massines, F.; Gouda, G. *J. Phys. D: Appl. Phys* **1998**, *31*, 3411.
[39] Massines, F.; Gherardi, N.; Fornelli, A.; Martin, S. *Surf. Coating Tech.* **2005**, *200*, 1855.
[40] Kogelschatz, U. *IEEE Transactions on Plasma Science* **2002**, *30*, 1400.
[41] Borra, J. P. *J. Phys. D: Appl. Phys* **2006**, *39*, R19.
[42] Borra, J. P. *Plasma Phys. Controlled Fusion* **2008**, *50*, 124036.
[43] Jidenko, N.; Jimenez, C.; Massines, F.; Borra, J. P. *J. Phys. D: Appl. Phys* **2007**, *40*, 4155.
[44] Goree, J. *Plasma Sources Sci. Technol.* **1994**, *3*, 400.
[45] Brunet P, R. R., Margot J, Massines F, Chaker M, *Plasma Process Polym* **2016.**, 9999:1.
[46] Bazinette, R.; Subileau, R.; Paillol, J.; Massines, F. *Plasma Sources Sci. Technol.* **2014**, *23*.
[47] Erdem, B.; Hunsicker, R. A.; Simmons, G. W.; Sudol, E. D.; Dimonie, V. L.; El-Aasser, M. S. *Langmuir* **2001**, *17*, 2664.
[48] Nur, H. *Materials Science and Engineering: B* **2006**, *133*, 49.